

Revealing Internal Heavy Chalcogen Atom Effect on the Photophysics of Dibenzo[*a,j*]phenazine-Cored Donor–Acceptor–Donor Triad

Shimpei Goto, Yuya Nitta, Nicolas Decarli, Leonardo Evaristo de Sousa, Patrycja Stachelek, Norimitsu Tohnai, Satoshi Minakata, Piotr de Silva,* Przemyslaw Data*, and Youhei Takeda*

S. Goto, Y. Nitta, Prof. Dr. N. Tohnai, Prof. Dr. S. Minakata, and Prof. Dr. Y. Takeda
Department of Applied Chemistry, Graduate School of Engineering, Osaka University
Yamadaoka 2-1, Suita 565-0871, Japan
E-mail: takeda@chem.eng.osaka-u.ac.jp

N. Decarli, Prof. Dr. P. Data
Faculty of Chemistry, Silesian University of Technology, M. Strzody 9, 44-100, Gliwice, Poland
E-mail: przemyslaw.data@polsl.pl

Dr. L. E. de Sousa, Prof. Dr. P. de Silva
Department of Energy Conversion and Storage, Technical University of Denmark, Anker Engelunds Vej 301, 2800 Kongens Lyngby, Denmark
E-mail: pdes@dtu.dk

Dr. P. Stachelek
Durham University, Chemistry Department, South Road, Durham DH1 3LE, United Kingdom

Prof. Dr. P. Data
Centre of Polymer and Carbon Materials, Polish Academy of Science, M. Curie-Skłodowskiej 34, 41-819, Zabrze, Poland

Abstract: A new twisted donor–acceptor–donor (D–A–D) multi-photofunctional organic molecule comprising of phenoselenazine as the electron-donors (Ds) and dibenzo[*a,j*]phenazine (DBPHZ) as the electron-acceptor (A) has been developed. The developed selenium-incorporated D–A–D compound is featured with multi-color polymorphism, distinct mechanochromic luminescence, chemically-stimulated luminochromism, thermally-activated delayed fluorescence, and room-temperature phosphorescence. The internal heavy atom effect on the photophysical properties of the D–A–D system has been investigated through the comparison with the physicochemical properties of a previously developed sulfur analogue and a tellurium analogue.

Introduction

Selenium (Se) and Tellurium (Te), that are heavier congeners of Sulfur (S), have a very similar and lower electronegativity (χ_P) with Sulfur (Se: 2.55, Te: 2.10, S: 2.58), respectively, and they have slight larger covalent radius than that of sulfur (Se: 1.17 Å, Te: 1.38 Å, S: 1.04 Å). Owing to such electronic and structural perturbation, the replacement of the S atoms of an organosulfur compound with Se or Te atoms leads to a drastic change in reactivity and physicochemical property. Such “internal heavy atom effect” have fascinated scientists, and indeed a myriad of functional organo-selenium and -tellurium compounds have been developed. Nowadays, they can find diverse applications in a range of fields such as biology,^[1] medicinal chemistry,^[1,2] chemical biology,^[3] synthetic chemistry,^[4] catalysis sciences,^[5] polymer sciences,^[6] and materials sciences.^[7]

In this context, planar π -conjugated molecules and polymers decorated with Se and/or Te at the main π -conjugated frameworks or at the peripherals of the π -systems have attracted considerable attention as functional materials for organic electronics. In addition to the intrinsic planar and rigid π -systems, the presence of Se/Te atoms results in not only strong intermolecular π -orbital interactions but also electrostatic interactions (i.e., chalcogen-bonding) in the solid states,^[8] allowing for efficient charge carrier transport. Thus, some classes of compounds, such as seleno-/telluroarenes, seleno-/tellurophenes, and their oligomeric and polymeric derivatives, have emerged as promising organic semiconducting materials, and they find applications in organic field-effect transistors (OFETs),^[9] organic photovoltaics (OPVs),^[10] and organic thermoelectronics (OTEs).^[11]

In stark contrast, organoselenium and organotellurium compounds displaying luminescence in the solid states have been less developed, and thereby the optoelectronic applications thereof are in their infancy.^[12] The incorporation of selenium and other heavy atoms such as halogens into a luminogenic scaffold often generates the pair of singlet excited state $^1(n,\pi^*)$ (S_1) and triplet excited state $^3(\pi,\pi^*)$ (T_1) or $^1(\pi,\pi^*)$ and $^3(n,\pi^*)$. In conjunction with the intrinsically large spin-orbit coupling (SOC) constant (ζ_{SO}) of Se (ca. 5.07 kcal/mol) and Te (ca. 11.3 kcal/mol),^[13] the SOC matrix element (H_{SOC}) for the S_1 – T_1 transition of a Se- or Te-containing π -conjugated compound becomes large, allowing the spin-forbidden S–T transitions.^[14] Therefore, upon photo-excitation, the T_1 state of an organoselenium/tellurium molecule is promptly populated through a rapid intersystem crossing (ISC) from the S_1 state.^[15] With a well-studied planar π -conjugated organoselenium/tellurium frameworks, the single-triplet energy splitting (ΔE_{ST}) is relatively large (>1 eV) comparable with other acene analogues, and as mentioned-above, the intermolecular interactions are strong in the solid states. As the results, the long-lived T_1 state in the solids would be just depopulated through non-irradiative pathways such as thermal internal conversion (IC) via bond rotations and molecular vibrations, and energy diffusion.

Over the last few years, the internal heavy atom effects on the optoelectronic properties of

triplet-harvesting organoselenium emitters based on twisted D- π -A^[16,17] and D- π -D^[18] scaffolds displaying thermally activated delayed fluorescence (TADF)^[19] and room-temperature phosphorescence (RTP)^[20] have been reported (Figure 1). In 2019, de Sa Pereira, Kukhta, and Lee investigated the effect of replacing Se for S atom of a D- π -A TADF emitter on the photophysics through a sophisticated time-resolved spectroscopic analysis of D_{Se}- π -A type compound **PSeZ-TRZ** (Figure 1a) in comparison with that of its sulfur TADF emitter **PTZ-TRZ**.^[16] The analysis of the complicated decays of **PSeZ-TRZ** in non-polar polymer matrix Zeonex[®] rationally explained the independent irradiative pathways of two conformers, i.e., quasi-axial (ax) and quasi-equatorial (eq) (Figure 1a). Most importantly, replacing Se for S does not affect the reverse ISC (rISC) in significant degree but so does room-temperature phosphorescence (RTP) efficiency of the donor. On the other hand, Credgington and Seferos investigated the effect of replacing Se for S of a TADF compound **TXO1-TPA** on ISC and rISC processes by developing a D- π -A_{Se} type compound **SeXO1-TPA** (Figure 1b).^[17] The detailed kinetic analysis revealed that the Se affects both of ISC and rISC rates, enhancing the ISC more than 250 times and the rISC 22 time faster than those of the sulfur TADF emitter. Given these apparently contradicting results, the position of Se atom on π -electron systems significantly affect the photophysical properties of the selenium-embedded compounds. Most recently, Kim and Lee developed D_{Se}- π -D_{Se} type metal-free RTP compounds **PSe1**, **PSe2**, and **PSe3** (Figure 1c) for OLEDs. The authors claimed that the n- π^* transitions involving differentially-oriented p orbitals on the Se atom ($p_z \rightarrow p_{xy}$) significantly enhance the spin-orbit coupling (SOC) element matrices between the S₀ and T₁, thereby accelerating the irradiation from the T₁ state.^[18] Zhao and Huang reported the effect of chalcogen atoms in the chalcogenophene- π -phenylcarbazoles on the optoelectronic properties and revealed dual emission behavior of fluorescence and RTP.^[21] He and co-workers developed a D-A_{Se}-D type organic phosphorescent compound for afterglow imaging and photodynamic therapy by taking the advantage of long-lived triplet excited states.^[22] Therefore, investigation on the effect of replacing Se/Te for S atoms of TADF/RTP-active compounds on their photophysical properties would provide profound insights into understanding the design principles for balancing conflicting factors ΔE_{ST} and SOC to realize novel chalcogen-containing organic photofunctional materials.

Herein we disclose the development of novel twisted donor-acceptor-donor (D-A-D) organic emitters **PSeZ-DBPHZ-PSeZ** and **PTeZ-DBPHZ-PTeZ** based on a new organoselenium/tellurium scaffold (D_{Se}-A-D_{Se} and D_{Te}-A-D_{Te}, respectively) (Figure 1d). Most importantly, the investigation of their physicochemical properties revealed that **PSeZ-DBPHZ-PSeZ** is multi-photofunctional material featured with polymorphs-dependent multi emission colors, single-molecular white emission (SMWE), and mechanochromic luminescence (MCL), chemical stimuli-responsive emission change, and distinct delayed emission in matrices and organic light-emitting

diodes (OLEDs) (Figure 1d). The comparison of the experimental properties and quantum chemical calculation data of the series of D–A–D compounds clarified that the conformational preference arising from the “ax” and “eq” donors is strongly correlated with the chalcogen atoms and thus governs their photophysical properties.

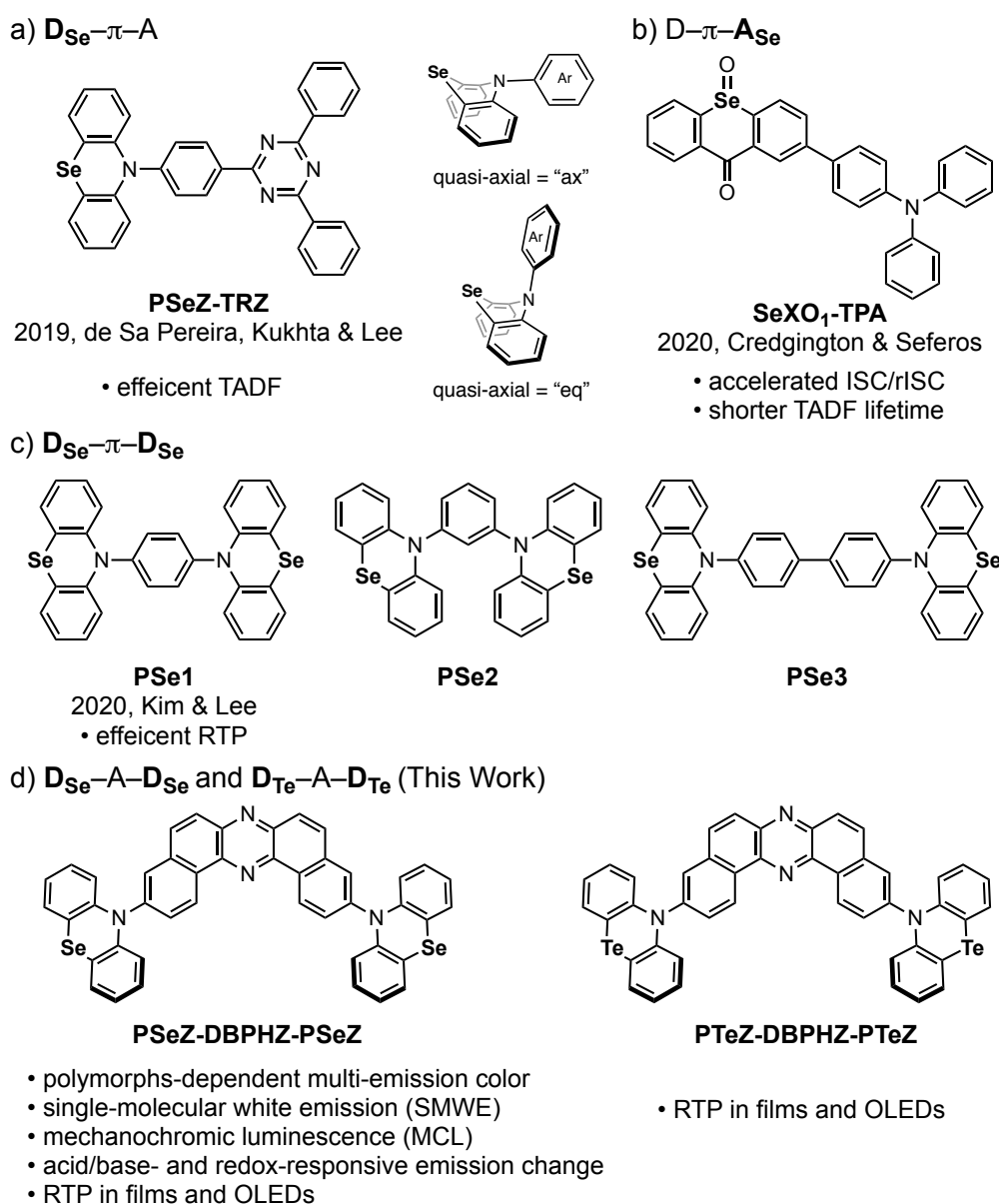
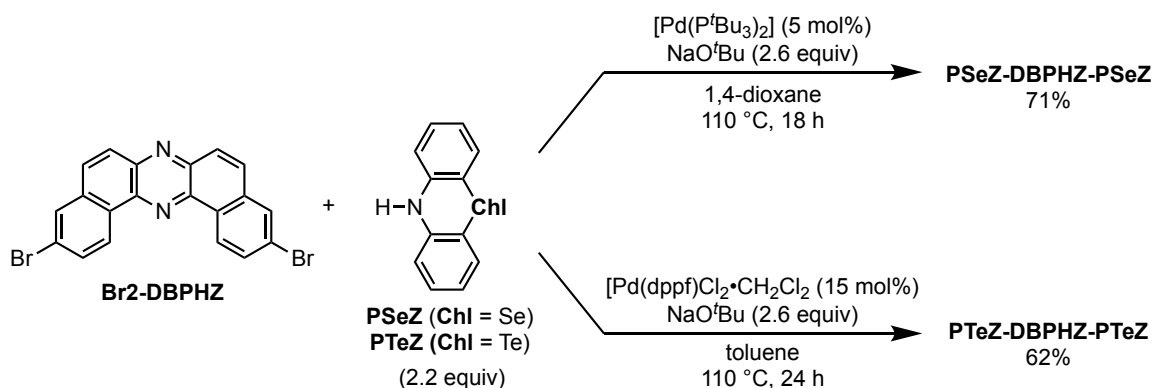


Figure 1. a)–c) Structures of previously reported TADF- and RTP-active organoselenium compounds; d) Structures of newly developed D–A–D type organoselenium and tellurium compounds.

Results and Discussion

Design and Synthesis. Previously, we have developed multi-photofunctional organic materials displaying thermally activated delayed fluorescence (TADF), mechanochromic luminescence (MCL),^[23] and room-temperature phosphorescence (RTP) properties, based on a donor–acceptor–

donor (D–A–D)^[24–29] or a D–A–D–A scaffold,^[30] utilizing dibenzo[*a,j*]phenazine^[31] as the key acceptor unit. In 2017, we reported the first example of TADF-active multi-color-changing MCL material (**PTZ-DBPHZ-PTZ**) based on the design concept of conformation-dictated regulation of luminescence properties, where the ax- and eq-conformer arising from the boat-chair geometry of phenothiazine plays the key role in giving divergent ground and excited state energies.^[26a] To reveal the effect of replacing Se/Te for S of **PTZ-DBPHZ-PTZ**, D–A–D compounds on the photo-functionality, **PSeZ-DBPHZ-PSeZ** and **PTeZ-DBPHZ-PTeZ** were designed (Figure 1d). **PSeZ-DBPHZ-PSeZ** was successfully synthesized through a Pd-catalyzed Buchwald-Hartwig double amination of 3,11-dibromo-dibenzo[*a,j*]phenazine (**Br2-DBPHZ**)^[31] with phenoselenazine (**PSeZ**) in a good yield (the upper equation in Scheme 1). The product was further purified through recrystallization from CH₂Cl₂/*n*-Hex solution to give yellow powdery solids. The product was fully characterized by ¹H, ¹³C, & ⁷⁷Se NMR, X-ray crystallography, mass spectroscopy, IR spectroscopy, and elemental analysis (for the details, see the SI). **PTeZ-DBPHZ-PTeZ** was also synthesized through an amination of **Br2-DBPHZ** with phenotellurazine (**PTeZ**) (the bottom equation in Scheme 1; for the details of synthesis and characterization, see the SI). In stark contrast to **PSeZ**, the known synthetic method for **PTeZ** is far from practical, due to the use of toxic mercury reagent.^[32] Therefore, we decided to establish an up-dated synthetic method for **PTeZ** by modifying our method for phosphorous-bridged diarylamine (dihydrophenophosphanizine).^[27] As the results, the cyclization of dilithiated *N*-Boc diarylamine with TeCl₄ followed by the reduction of the resulting Te(IV) center successfully gave **PTeZ** (for the detail procedures, see the SI). Incidentally, during the preparation of this manuscript, the Patureau group also reported a robust synthetic method for **PTeZ** using Te(0) as the tellurium source.^[33] It is noted that **PTeZ-DBPHZ-PTeZ** represents the first example of D–A type emissive compounds that have phenotellurazine (**PTeZ**) as the electron donor.



Scheme 1. Synthesis of **PSeZ-DBPHZ-PSeZ** and **PTeZ-DBPHZ-PTeZ**.

Polymorphisms. Through our attempts to recrystallize **PSeZ-DBPHZ-PSeZ** from various solvent systems, we serendipitously found out that the molecule forms 3 different concomitant polymorphs (denoted as **G**, **Y**, and **O**) grown from the same *n*-Hex/EtOAc solution. Notably, those polymorphs displayed distinctly different photoluminescence colors (green, yellow, and orange) under the irradiation of a UV light (Figure 2a). As the results of screening of solvent systems for selective preparation of those polymorphs, we found out that the recrystallization from a CHCl₃/*n*-Hex solution exclusively gave polymorph **Y**, while CH₂Cl₂/AcOEt solvent system provided polymorph **O**. The characterization of these polymorphs obtained from different solvent systems were confirmed by the identification of experimental and simulated powder X-ray diffraction (PXRD) patterns. Unfortunately, we were not able to find solvent system to exclusively provide polymorph **G** after extensive attempts. The PL spectra of polymorphs **Y** and **O** clearly show significant difference in emission profiles (^Yλ_{em} 546 nm, ^YΦ_{PL} 0.02; ^Oλ_{em} 666 nm, ^OΦ_{PL} 0.03) (Figure 2b). Due to the scarcity of the amounts of the **G** polymorphs, the PL spectra were not collected. To investigate the origin of the significant difference in emission colors of those polymorphs, the X-ray crystallographic analyses were conducted (Figure 2c–k). Unexpectedly, the emission difference stems from not only the different conformational geometries (i.e, **G**: ax-ax conformer; **Y** and **O**: eq-ax conformers, Figure 2c–e) but also the different packing modes (Figure 2f–k). In all the polymorphs, anti-parallel dimeric pairs were found with close interplane distance (*d*_{inter}) between the two adjacent DBZPH units (*d*_{inter} 3.27–3.47 Å), which cancel out dipole moments (Figure 2i–k). Close look at the packing structures of **Y** and **O** revealed the distinct difference in *d*_{inter} and the degree of overlap of the π unit of the acceptor (DBPHZ) (Figure 2j and k). From the comparison with the packing structure of previously-reported sulfur-analogue **PTZ-DBPHZ-PTZ** in orange emitting single crystal (eq-ax conformation, λ_{em} 640 nm),^[26a] it turned out that the packing structure of the selenium D–A–D compound in polymorph **O** is very similar to that of **PTZ-DBPHZ-PTZ** in the orange-emitting crystal, where the overlap of the π-unit in the dimeric pair and *d*_{inter} (3.46 Å) is almost the same. Taken together, we can conclude that the difference in emission profiles among the polymorphs of **PSeZ-DBPHZ-PSeZ** are not only determined by the molecular conformations but also the intermolecular electronic interactions.^[34]

In contrast to the selenium D–A–D compound, any single crystals of tellurium containing compound **PTeZ-DBPHZ-PTeZ** suitable for X-ray crystallographic analysis were not obtained even after many attempts, due to powdery nature of the compound.

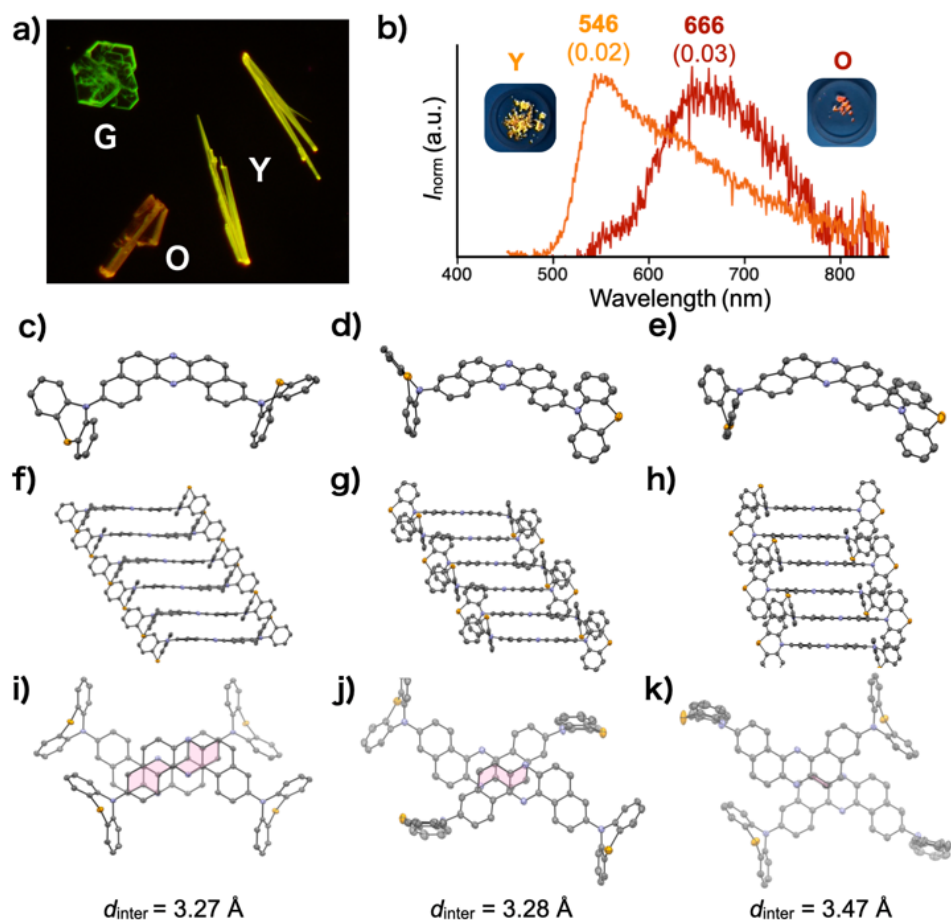


Figure 2. a) A photograph of concomitant polymorphs **G**, **Y**, and **O** under the irradiation of a UV lamp ($\lambda = 365$ nm); b) PL spectra of **Y** and **O** ($\lambda_{\text{ex}} = 340$ nm; values in parentheses indicate the PLQY determined with an integral sphere); molecular structures of **PSeZ-DBPHZ-PSeZ** in c) **G**, d) **Y**, and e) **O**; packing structures of **PSeZ-DBPHZ-PSeZ** in f) **G**, g) **Y**, and h) **O**; dimeric pairs of **PSeZ-DBPHZ-PSeZ** with the closest d_{inter} value in i) **G**, j) **Y**, and k) **O** polymorphs. The pale pink region indicates the overlap area of π -moieties.

Steady-state photophysical properties in solutions. To clarify the single molecular photophysical properties of the D–A–D compounds, the steady-state photophysical properties of dilute solutions ($c = 10^{-5}$ M) in various solvents were investigated (Figure 3 and Table 1). Surprisingly, the Se-containing compound **PSeZ-DBPHZ-PSeZ** in dichloromethane displays a quite different absorption spectrum from the superposition of the individual spectra of D (**PSeZ**) and A (**DBPHZ**) (2D +A, Figure 3a). The disappearance of the vibronic absorptions (ca. λ 300 nm and 380–420 nm) derived from the acceptor unit indicates a strong electronic coupling between the D and A units (Figure 3a). This implies a quite different conformation of the Se compound from its sulfur analogue, where eq-eq conformer dominates and efficiently electron-decoupled absorption spectra displays.^[26a] In a similar manner with our previously developed DBPHZ-cored D–A–D compounds,^[25–29] an intramolecular charge-transfer (ICT) transition at around λ 460 nm was observed (Figure 3a). However, when compared to the

absorption spectra of the sulfur analogue, the molar coefficient (ca. ϵ 25,000–28,000) of the ICT band of the selenium compound is much larger than that of sulfur compound (ca. ϵ 10,000).^[26a] A similar trend in the absorption spectra was observed for tellurium-containing compound **PTeZ-DBPHZ-PTeZ**, where more distinct vibronic structure in the lowest-energy absorption regime ranging from 420 to 480 nm was dominated than the selenium compound (Figure S4). This distinct difference caused by the Se and Te replacement for S atom suggests the ax-ax conformer is more dominated than sulfur analogue in solutions, which was supported by the theoretical calculations (*vide infra*). The comparison of the conformational population of the D–A–D compounds with each chalcogen-bridged diarylamine donor (S, Se, and Te) is illustrated in Figure 3b. The effect of Se replacement for S in the D–A–D scaffold includes the switching of the majority conformer from eq-eq (ca. 59% contribution for the sulfur compound) to ax-ax (ca. 55% contribution for the selenium compound; ca. 98% contribution for the tellurium compound, Tables S5 and S6). Importantly, energy decomposition analysis (EDA)^[35] shows that the conformational preference results from an interplay between Pauli, electrostatic, and orbital relaxation factors (Table S10). All these terms are strongly coupled to the equilibrium geometry. Nevertheless, substituting S with Se and Te in the D–A–D scaffold at a fixed geometry always leads to the relative stabilization of the axial conformer by Pauli repulsion and its destabilization by electrostatic and orbital relaxation. Given that the destabilizing Pauli energy accounts for electronic repulsion, the thermodynamic preference of ax-ax conformers over eq-eq conformers in the selenium and tellurium-containing D–A–D compounds would be rationalized by less transannular electronic repulsion between the lone pairs on the N and the chalcogen atoms in the boat-chair donor unit.

The absorption spectra of **PSeZ-DBPHZ-PSeZ** were not affected by solvent polarity, suggesting the almost constant distribution of the conformers (dotted lines, Figure 3c). The weak effect of solvent polarity on the conformer distribution is also confirmed by theoretical calculations as shown in Table S7. The difference in the absorption spectra between S, Se, and Te-containing D–A–D compounds is also fully explained by different conformer stability. The theoretical spectra calculated by weighting contributions from all the conformers agree with the experiments in terms of both relative band positions and their intensities (Figure S16).

Not only the absorption, the impact of the Se replacement was drastic in photoluminescence (PL) spectra as well. Most importantly, the toluene solution of **PSeZ-DBPHZ-PSeZ** displayed a dual emission peaked at λ 480 nm and 644 nm, thereby giving white emission (the photograph in Figure 3c). This is a remarkable contrast with the sulfur compound: it only gives a broad Gaussian-type CT emission at around λ 657 nm in toluene.^[26a] This should be associated with the dominance of the orthogonally-structured conformers (eq-eq and eq-ax) in the sulfur compound, which generates distinctly charge-separated CT excited states and relaxed in a polar solvent. The Se replacement affects

the thermodynamic stability of the conformers, and thereby the admixture of the greenish LE emission at around λ 480 nm from the dominant ax-ax conformer and the CT emissions from eq-ax (~38%) and eq-eq (~8%) conformers should yield white emission. Recently, single molecular white emitters (SMWEs) have emerged as promising materials for optoelectronic and sensor applications.^[36] Nevertheless, the rational design of SMWEs is difficult, due to the energy transfer problems, for instance. Therefore, the introduction of **PSeZ** donors in D–A–D scaffold allows for strategic design of SMWEs by mixing ax-ax and eq-based conformers to balance energetically-different emissions. As the polarity of solvent increases, the LE emission at around 480 nm in toluene gradually red-shifted, while the CT emission at around 650 nm in toluene was totally vanished (Figure 3c). This polarity-dependence would support the significant difference in CT natures of the two emissions observed in toluene: the bluer emission is LE with a weak CT nature yielded from ax-ax conformer, while redder emission is derived from a stabilized CT excited state with a highly twisted structure (twisted intramolecular charge-transfer: TICT state) from eq-ax and eq-eq conformers. Due to the distinct charge separation, the redder emission is highly susceptible to solvent polarity, and in more polar solvent than toluene, the lower CT excited state is dissipated through atomic vibrations and rotations, following the energy gap law. Theoretical calculations reveal that strong stabilization of the S_1 state in eq-ax and eq-eq conformers is due to the planarization of the equatorial donor unit in the excited state (Figure S15). Such CT state is further stabilized by the dielectric response of the solvent; the calculated emission wavelength in toluene is 558 nm (2.22 eV) for eq-ax and 608 nm for eq-eq (2.04 eV) (Table S8). In a polar THF solvent, the CT emission are predicted at 656 nm (1.89 eV) and 720 nm (1.72 eV), respectively, but these states are most likely relaxing non-radiatively.

Tellurium-incorporated D–A–D compound **PTeZ-DBPHZ-PTeZ** shows fluorescence with a low quantum yield (Φ_{PL} 0.01–0.15) in diluted organic solutions, showing positive solvatochromic luminochromism (Figure S4 and Table S4). In contrast to **PSeZ-DBPHZ-PSeZ**, the tellurium compound did not show dual emission in toluene, which is in good agreement with the domination of ax-ax conformer in this solvent (Figure 3b) as suggested by the theoretical calculation (*vide infra*).

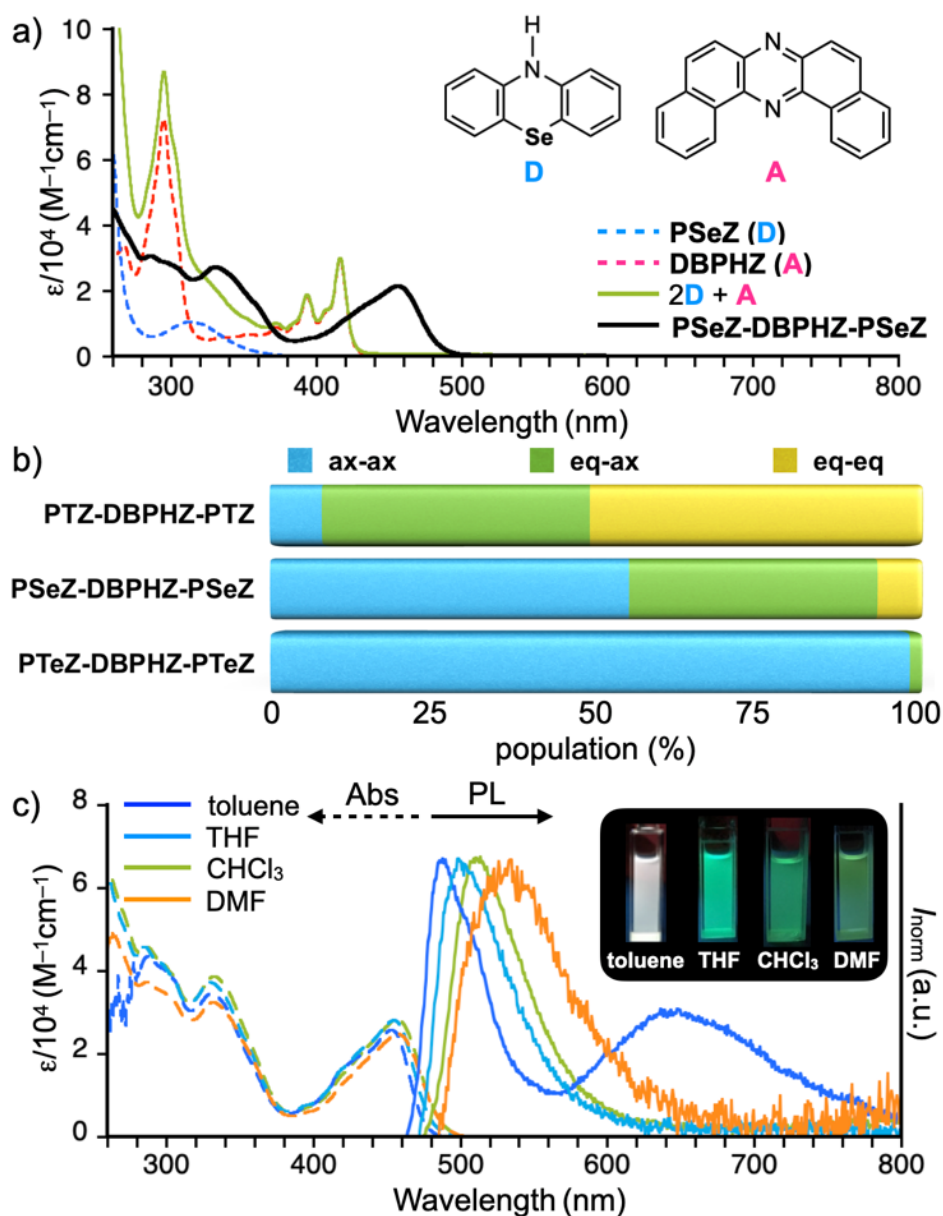


Figure 3. a) Steady-state UV-vis absorptions of DCM solutions ($c = 10^{-5}$ M) of PSeZ (cyan dotted line), DBPHZ (pink dotted line), 2D+A (moth solid line), and PSeZ-DBPHZ-PSeZ (black solid line); b) Conformational population of D-A-D compounds with S, Se, and Te donors in vacuum; c) Steady-state UV-vis absorption and photoluminescence (PL) spectra of solutions ($c = 10^{-5}$ M, $\lambda_{ex} = 400$ nm) of PSeZ-DBPHZ-PSeZ prepared from various solvents. The inset photographs indicate the solutions taken under the irradiation of a UV light ($\lambda = 365$ nm).

Table 1. Summary of steady-state photophysical properties of PSeZ-DBPHZ-PSeZ in solutions ($c = 10^{-5}$ M).

solvent	λ_{abs} [nm]	ε [M ⁻¹ cm ⁻¹]	λ_{em} [nm]	$\Phi_{\text{PL}}^{[a]}$
Toluene	453	25,800	480, 644	0.04
THF	454	28,200	493	0.01
CHCl ₃	456	28,400	504	0.02
DMF	457	24,900	520	0.01

[a] Determined with an integrating sphere.

Mechanochromic Luminescence (MCL) properties. The photoluminescence behavior of **PSeZ-DBPHZ-PSeZ** under external stimuli was then investigated (Figure 4). The as-prepared sample is a powdery crystalline sample, which shows sharp diffraction patterns in PXRD measurement (Figure S6a). Upon the irradiation of UV light, the solid emits yellow PL (λ_{em} 576 nm, Φ_{PL} 0.04) (the inset photograph, Figure 4a). Upon grinding the solid with a pestle and a mortar, the emission color drastically turned to deep-red, displaying a broad Gaussian emission spectrum (λ_{em} 671 nm, Φ_{PL} 0.09). (the inset photograph, Figure 4a). The ground sample was found amorphous from the PXRD analysis (Figure S6a). At a glance, this mechanochromic luminescence (MCL) behavior is very similar to that of its sulfur analogue.^[26a] However, the response against thermal and vapor treatment of the ground Se-compound was found quite different from its sulfur atom (Figure 4a). Upon heating the red-emitting ground sample on a hot plate at 200 °C for 15 min, the emission color reverted back to yellow, which was clearly seen on the PL spectra (Figure 4a). The PXRD patterns of the heated sample were found almost superimposed with those of the as-prepared powder sample (Figure S6a), confirming the recovery of the initial state. The fuming of the ground sample with organic vapor such as AcOEt and CHCl₃ also caused the similar recovery of yellow emission (Figure S5). The PXRD analysis supported the recovery of the initial state (Figure S6a). The deep-red emitting amorphous state was reproduced by grinding the heated and fumed samples. In contrast, the amorphous state of the sulfur analogue **PTZ-DBPHZ-PTZ** shows a much smaller blue-shift for heating (621 cm⁻¹) and fuming (1920 cm⁻¹)

than that for selenium-compound (2458 cm^{-1}), and the deep-red emitting (ground sample) state does not revert back to yellow-emitting state.^[26a] Therefore, the Se replacement for S atoms allows for high reversibility of the two-emitting states. To obtain deeper insights on this unique phenomenon, we compared the PXRD patterns of the yellow-emitting crystalline sample with those predicted from the single-crystals of **G**, **Y**, and **O** (Figures S6b). The comparison suggested that the eq-ax conformer would be the conformer contained in the yellow-emitting powder solids. Differential scanning calorimetry (DSC) of each solid sample revealed that the only the ground orange-emitting sample shows exothermic peaks at around 159 and 198 °C (Figure S7), suggesting the ground sample is meta-stable state. Therefore, we can conclude that the enhanced reversibility of the initial state would be associated with the thermodynamic stability of the eq-ax conformer over eq-eq conformer in the aggregate states. Although this thermodynamic conformational preference appears to be inconsistent with that in solutions (Figure 3b), there could be many factors controlling the thermodynamic preference of conformers in the solid states such as packing forces and intermolecular interactions.

In addition to the reversible MCL behavior in response to various stimuli, the selenium compound shows response to chemical stimuli. For example, the photoluminescence (PL) of the as-prepared **PSeZ-DBPHZ-PSeZ** turns off upon the treatment of vapor of trifluoroacetic acid (TFA), while the yellow PL turns on by fuming the solid with basic triethylamine (TEA) vapor (Figure S8a). This turn/on-off cycle is reversible and repeatable (Figure S8b). The selenium compound also shows redox-responsive emission color change through the reversible manipulation of the oxidation state of the Se atoms (i.e., $\text{Ar}_2\text{Se} \rightleftharpoons \text{Ar}_2\text{Se=O}$) (Figure 4b, for the details of the redox procedures, see the SI). It is worth mentioning that such Se-oxidation caused drastic change in absorption spectra, where the vibronic absorptions ascribed to the acceptor unit (ca. λ_{abs} 390 and 420 nm) are manifested and the CT absorption at around 450 nm is decreased (Figure 4b) when compared to those of **PSeZ-DBPHZ-PSeZ** (Figure 3c). The photoluminescence of the oxidized form (**PSeOZ-DBPHZ-PSeOZ**) displays more CT character showing larger positive solvatochromic shift (Figure 4b) than that of Se(II) species (Figure 3c), although the electronic donating ability of the phenoselenazine unit should be decreased. A possible rationale for explaining these contradicting spectra change would be that the effect of the Se-oxidation caused drastic change in conformational preference from ax-ax to eq-based conformers, where the D and A units are almost completely decoupled, and thereby the charge-separated excited states are stabilized by the perpendicular D–A–D scaffold.

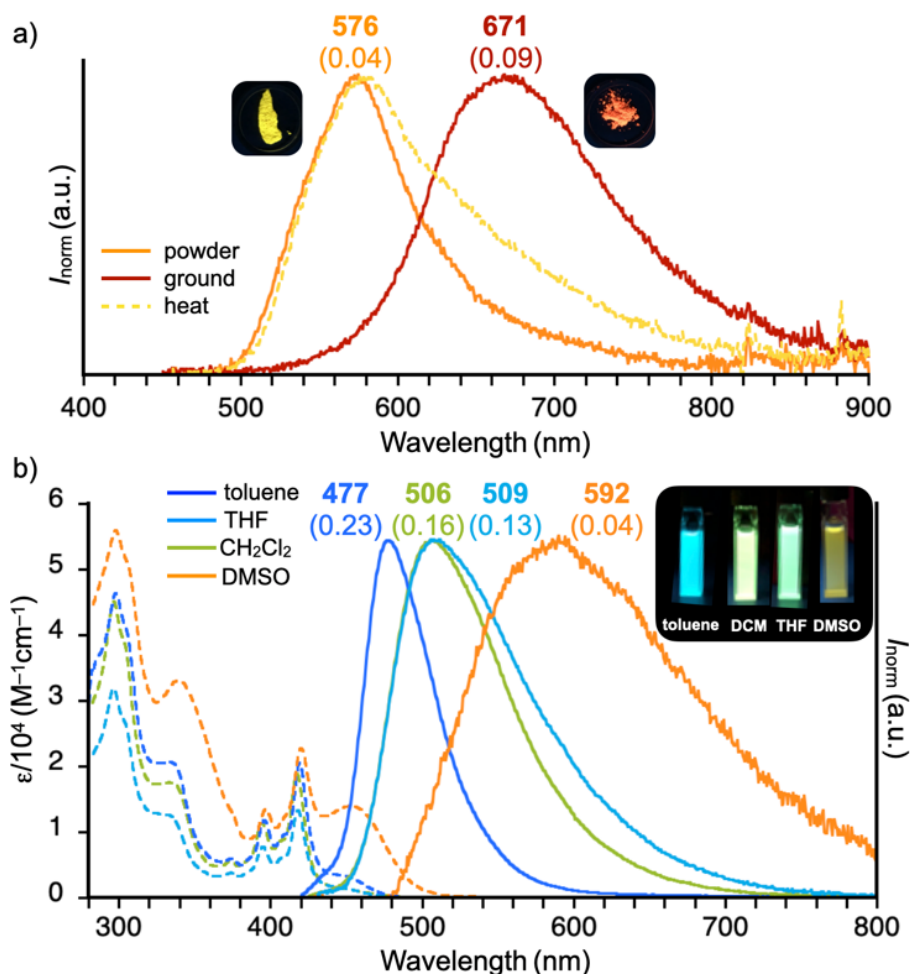


Figure 4. a) Steady-state PL spectra of solids of powder (as prepared), ground, and heated samples; b) Steady-state UV-vis absorption and photoluminescence (PL) spectra of solutions ($c = 10^{-5}$ M, $\lambda_{\text{ex}} = 400$ nm) of **PSeOZ-DBPHZ-PSeOZ** prepared from various solvents. The inset photographs indicate the solutions taken under the irradiation of a UV light ($\lambda = 365$ nm).

In contrast to the behavior of the selenium compound, **PTeZ-DBPHZ-PTeZ** did not show photoluminescence in the solid state, probably due to the rapid ISC and IC accelerated by larger SOC in the condensed state. Although the D–A–D tellurium compound does not show PL in the aggregated solid states, the compound exhibits blue-greenish PL in matrices with a long lifetime, indicating the room-temperature phosphorescence (RTP) (for the details, see the following time-resolved spectroscopy section). More interestingly, the phenotellurazine donor (**PTeZ**) shows yellow (λ_{em} 556 nm, Φ_{PL} 0.09) and orange (λ_{em} 591 nm, Φ_{PL} 0.19) photoluminescence (PL) in the solid states (Figure S9a) and Zeonex[®] matrix (Figure S9b), respectively. The unexpected orange emission in the matrix was characterized with a long lifetime (τ_{avr} 11.7 μs under vacuum, Figure S9c), which becomes shorter under the effect of air (τ_{avr} 5.7 μs , Figure S9c). Given this emission peak almost matches with that of

phosphorescence spectra acquired at 77 K (Figure S9b), the orange emission from **PTeZ** should be RTP. Although the details of the origin of this unique RTP awaits further analysis, the large SOC, which was supported by the theoretical calculation ($\langle S_0 | H_{\text{SOC}} | T_1 \rangle$ 13.51 cm⁻¹, Table S13), should accelerate the irradiation from the T_1 to the S_0 state. It should be noted that **PTeZ** represents a new entry to organotellurium RTP family.^[37]

Time-resolved Spectroscopic Analysis. Initial steady-state photoluminescence analysis revealed the possibility of room-temperature phosphorescence (RTP) of both D–A–D compounds. Nevertheless, the full time-resolved analysis was indispensable to fully proof the photophysical mechanism. For that purpose, we investigated the photophysical properties of the solid-state layers of **PSeZ-DBPHZ-PSeZ** and **PTeZ-DBPHZ-PTeZ** in both a non-polar polymeric host Zeonex[®] and small molecular host CBP [4,4'-bis(*N*-carbazolyl)-1,1'-biphenyl] (Figure 5). As supporting work, the analysis of pure donors (**PSeZ** and **PTeZ**) in Zeonex[®] matrix was also investigated (Figure S14). The layers were deposited on sapphire substrate and analyzed in broad range of temperatures from 10 K up to 300 K. The short-lived emission of **PSeZ-DBPHZ-PSeZ** in Zeonex[®] matrix observed at 5.1 ns could be associated with emission from S_1 (¹LE) state and is similar at low (80 K, black line in Figure 5a) and room-temperature (300 K, blue line in Figure 5a). At further time delay, the emission is shifted to lower energies, and the phosphorescence is observed at low temperature (red line in Figure 5a). As the temperature rises, the delayed emission is hypsochromically shifted, and the spectrum becomes broader (green and purple lines in Figure 5a). Based on theoretical calculation, the ΔE_{ST} gap of **PSeZ-DBPHZ-PSeZ** in an ax-ax form is larger (490 meV) than the gap between T_1 and T_2 states ($\Delta E_{T_1-T_2}$ = 400 meV) (Figure 7). Given these energy alignments and the SOC between the S_0 – T_2 states (1.56 cm⁻¹), the temperature activated process (Figure 5a and e) could be related with the processes comprising of ISC (from S_1 to T_1) followed by thermal reverse internal conversion (from T_1 to T_2) and the photo-irradiation from the T_1 and/or T_2 states.^[29] Given the **PSeZ-DBPHZ-PSeZ** is admixrue of ax-ax and eq-ax conforms (Figure 3b), the energy transfer from the triplet excited state of ax-ax conformer to eq-ax conformer followed by TADF emission from the ¹CT state would also likely to occur.

Slightly different and complex behavior was observed for the **PTeZ-DBPHZ-PTeZ** in Zeonex[®] (Figure 5b). The emissions at short delay times (in the ns region) are related with the emission from the S_1 (black and blue lines in Figure 5b). As for the long-delayed emission (phosphorescence), the emission slightly shifted to the higher energy regime with the rise of temperature (red and green lines in Figure 5b). Interestingly, while the energy level and the spectrum shape of the phosphorescence from T_1 of **PSeZ-DBPHZ-PSeZ** are similar to those of previously studied DBPHZ-cored D–A–D compounds,^[24-29] the phosphorescence of **PTeZ-DBPHZ-PTeZ** appears to be much more similar to the phosphorescence of donor (**PTeZ**) (Figure S14b). But, the calculation suggests that similarity is

coincidental. The T_1 state of the dominant ax-ax conformer of **PTeZ-DBPHZ-PTeZ** is localized on the acceptor (${}^3\text{LE}_A$), and the donor retains its bent structure (Figure 7f), while the T_1 state of **PTeZ** has a planarized geometry which stabilizes the excited state (Figure S17). In the ax-ax conformer of the D-A-D compound, such planarization is not possible, due to the steric repulsion between D and A units. As the results, the energies of both triplet emissions of D and D-A-D compounds appear to be very close to each other.

More difficult processes to evaluate are involved in the photophysical properties of the investigated compounds inside CBP host, which was used for the fabrication and evaluation of OLED devices (Figure 5c, d, g, and h). The emissions of both D-A-D compounds at shortest times are similar to those in Zeonex[®] matrix and should be ascribed to the localized excited singlet state (${}^1\text{LE}$) in both low (80 K, black lines in Figure 5c and d) and room temperature (300 K, blue lines in Figure 5c and d). With both compounds, at low temperatures and long delay times, the phosphorescence is observed in the lower energy region than those in for Zeonex[®] layers, but the intensity is not that significant, suggesting it could be the emission from the lowest CT state. On one hand, the thermally activated emission processes are on the same energy levels like the process from the lowest ${}^3\text{LE}$ state, but the spectra are broader like the emission related to charge transfer process (Figure 5c, d, g, and h). Such complex behavior is not usually observed, but as mentioned before, we probably observe the emission from T_1 and a higher triplet state (T_2).^[29] The change of the host more affects the CT excited state energies to the lower level than LE states, thereby in CBP host both D-A-D compounds display almost the same energy level.

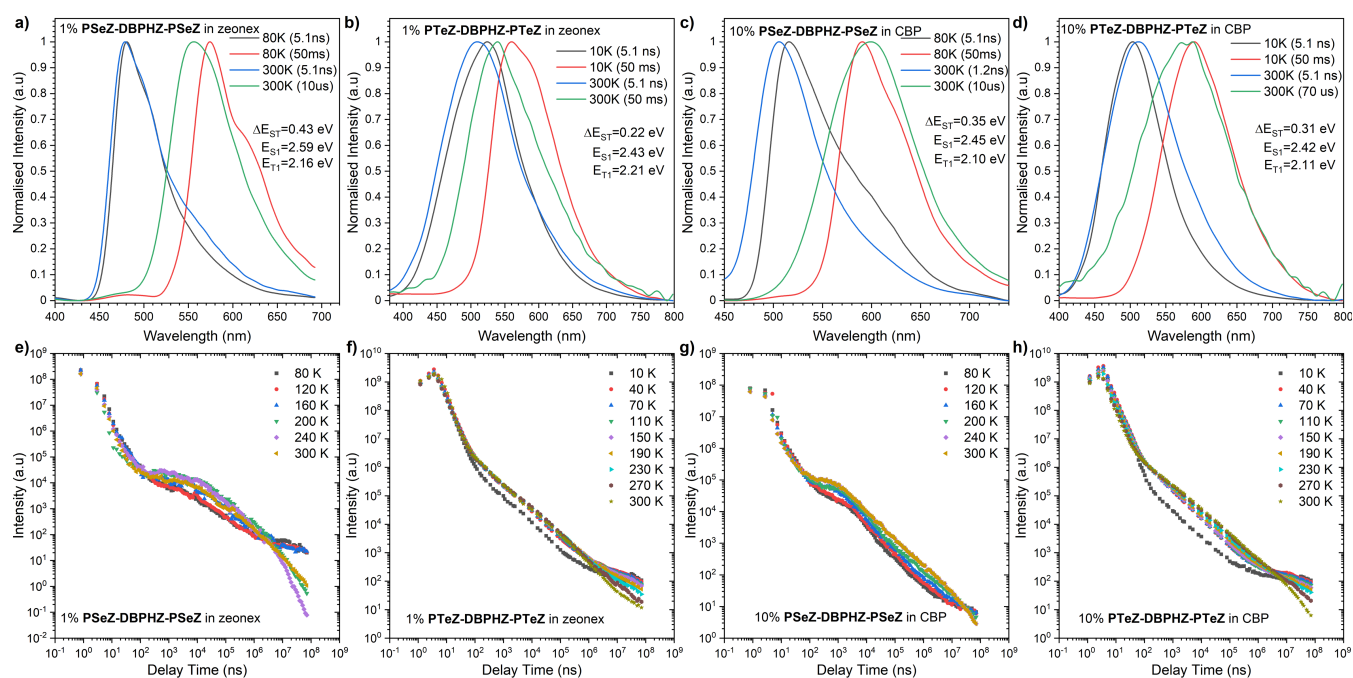


Figure 5. Time-resolved spectroscopic analysis of **PSeZ-DBPHZ-PSeZ** and **PTeZ-DBPHZ-PTeZ** in matrices: Photoluminescence spectra of a) **PSeZ-DBPHZ-PSeZ** and b) **PTeZ-DBPHZ-PTeZ** in Zeonex[®]; c) **PSeZ-DBPHZ-PSeZ** and d) **PTeZ-DBPHZ-PTeZ** in CBP; Photoluminescence decay of e) **PSeZ-DBPHZ-PSeZ** and f) **PTeZ-DBPHZ-PTeZ** in Zeonex[®]; g) **PSeZ-DBPHZ-PSeZ** and h) **PTeZ-DBPHZ-PTeZ** in CBP.

OLED fabrication and characterization. The electrochemical behavior of the donors and D–A–D compounds in dichloromethane was investigated with cyclic voltammetry (CV) (Figure S12). The cyclic voltammogram of **PSeZ-DBPHZ-PSeZ** displayed a reversible oxidation and reduction curves at $^{\text{ox}}E_{\text{onset}} = +0.31$ V and $^{\text{red}}E_{\text{onset}} = -1.71$ V (vs. Fc/Fc^+ redox couple), respectively. This electrochemical behavior looks typical for DBPHZ-cored D–A–D compounds (Figure S12a).^[24–29] On the other hand, the tellurium compound **PTeZ-DBPHZ-PTeZ** showed irreversible electrochemical redox behavior (Figure S12b), indicating the less electrochemical instability than the sulfur^[26a] and selenium analogues. Such tendency in the electrochemical analysis was previously reported in thiophene, selenophene, and tellurophene analogues, where the decomposition of the tellurophene ring was observed during the oxidation process.^[38] When compared to the donors (**PSeZ** and **PTeZ**), distinct positive shift in the oxidation potential for the both D–A–D compounds by >0.3 V was observed (Figure S12). The ionization potential (IP) and electron affinity (EA) for the **PSeZ-DBPHZ-PSeZ** and **PTeZ-DBPHZ-PTeZ** estimated from the CV experiment were estimated to be 5.41/3.39 eV and 5.38/3.35 eV, respectively.^[39] When compared to the IP/EA of the sulfur analogue **PTZ-DBPHZ-PTZ** (5.33 eV/3.38 eV)^[26a] and oxygen analogue **POZ-DBPHZ-POZ** (5.36 eV/3.38 eV),^[25] the Se/Te replacement effect for S atoms in the D–A–D scaffold on electrochemical redox characters is very small. This can be explained by the kinetic process: the conformer with the lowest oxidation/reduction potential (eq-eq) is faster electrochemically oxidized/reduced on the electrode than other conformers (eq-ax and ax-ax) with higher oxidation/reduction potentials. What is also interesting, both D–A–D compounds undergo oxidative electropolymerization process after the third oxidation peak (Figure S13a and b). It is also noted that only **PTeZ** donor forms polymer on the electrode (Figure S13c).

The thermogravimetry analysis (TGA) revealed their high thermal stability [**PSeZ-DBPHZ-PSeZ**: T_g (5 wt%) 383 °C under N_2 gas; **PTeZ-DBPHZ-PTeZ**: T_g (5 wt%) 412 °C under N_2 gas]. This indicates the feasibility of thermal sublimation process of OLED devices under vacuum (Figure S10 and S11). The investigated compounds were used as dopant in the CBP matrix. The following two OLED structures were deposited using high-vacuum thermal evaporators, Dev1: ITO/NPB (40 nm)/10% **PSeZ-DBPHZ-PSeZ** in CBP (25 nm)/TPBi (50 nm)/LiF (1 nm)/Al (100 nm); Dev2: ITO/NPB (40 nm)/10% **PTeZ-DBPHZ-PTeZ** in CBP (25 nm)/TPBi (50 nm)/LiF (1 nm)/Al (100 nm).

The performances and photophysical results of the fabricated OLED devices were investigated and compared in order to evaluate emissive pathways that boost the efficiency properties. Most importantly, dual-emissive property of the emitters was manifested in both OLED devices (Figure 6a). Such behavior is not usual, but taking into the time-resolved spectroscopic analysis data (Figure 5), the higher-energy emission at around λ_{em} 500 nm in both cases would be related with the electroluminescence from the S_1 (1LE) state and the lower-energy emission at around λ_{em} 600 nm with the RTP from the 3LE state. In other words, fluorescence and room-temperature phosphorescence (RTP) processes are involved in the electroluminescence.^[40] In both cases, the RTP contribution in overall emission, which was estimated from the comparing the area of emission spectra acquired in aerated and degassed conditions, is higher than 90%, and therefore the mostly related factor for the efficiency of the device should be the phosphorescence process. The highest external quantum efficiency (EQE) of the OLEDs was obtained with **PSeZ-DBPHZ-PSeZ** (4.35%), where the device with tellurium derivative **PTeZ-DBPHZ-PTeZ** showed a lower EQE of 1.89% (Figure 6c). These EQE values may not be that high, when compared with the OLED devices with existing heavy-atom-containing RTP organic emitters. But, if we assume that the overall PLQY for those compounds is less than 10%, it would suggest we obtained as highest efficiency as possible. On the other hand, the devices exhibit quite high luminance as for selenium and tellurium derivatives with up to 10,000 cd/m² for **PSeZ-DBPHZ-PSeZ** and more than 4,000 cd/m² for **PTeZ-DBPHZ-PTeZ**-based device.

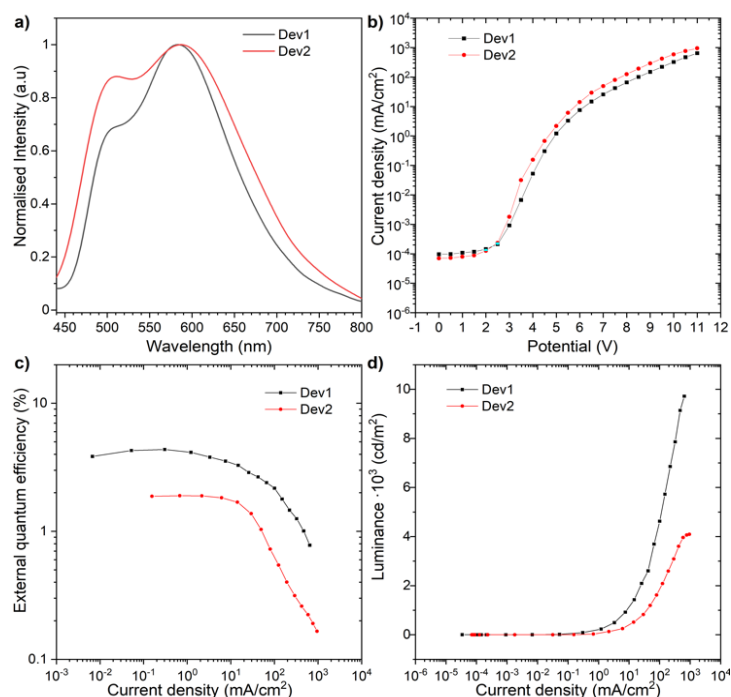


Figure 6. The characteristics of the OLED devices: a) Electroluminescence spectra; b) Current density-bias characteristics; c) EQE-current density characteristics; d) Luminance-current density characteristics.

Theoretical Calculations. To obtain deeper insights into the developed emitters, theoretical calculations were performed at the density functional theory level for the **PSeZ-DBPHZ-PSeZ** and **PTeZ-DBPHZ-PTeZ** compounds (see SI for details). Ground state geometry optimizations of the different conformers associated with a weighting procedure using Boltzmann factors at 300 K allowed us to conclude that all the three **PSeZ-DBPHZ-PSeZ** conformers (i.e., ax-ax, ax-eq, and eq-eq) should coexist at room temperature under vacuum, with the ax-ax conformation being the most stable (55% probability), followed by eq-ax (38%) and eq-eq (7%). In contrast, only two **PTeZ-DBPHZ-PTeZ** conformers are expected to be present at room temperature, namely ax-ax (98%) and eq-ax (2%). As such, we notice that one of the effects of heavy atom substitution from S to Se and Te is a progressive dominance of ax-ax conformations (Figure 3b), due to the deepening of the potential energy surface in this particular geometry. Importantly, conformational preference is not significantly affected by solvents, as shown in Table S7.

Excited state calculations in toluene revealed that for all **PSeZ-DBPHZ-PSeZ** conformers the T_1 states correspond to a localized excitation (3LE_A) state of the acceptor unit. On the other hand, S_1 states correspond to charge transfer (CT) states in all but the ax-ax conformer, as evidenced by the natural transition orbitals (NTOs) presented in Figure 7a, b, and c. However, Figure 7d, e, and f show that for eq-ax and ax-ax **PTeZ-DBPHZ-PTeZ** conformers, both S_1 and T_1 states correspond to localized excitations in the acceptor portion of the molecule, whereas the eq-eq conformer presents an S_1 state with CT character and a T_1 state that is localized in the donor unit. In particular, this difference is reflected in the significantly higher oscillator strength associated with S_0 - S_1 transitions of the **PTeZ-DBPHZ-PTeZ** molecule. In fact, the S_0 - S_1 transitions for both the eq-eq and eq-ax conformations of **PSeZ-DBPHZ-PSeZ** are predicted to be forbidden (zero oscillator strength). These characteristics, in addition to the aforementioned population of the different conformers, account for the observed differences in the absorption spectrum of the S, Se and Te-containing D-A-D compounds.

Calculated emission energies from the S_1 state in the ax-ax conformers of both compounds predict fluorescence at around 2.5 eV, in agreement with experimental results. A lower energy band in **PSeZ-DBPHZ-PSeZ** fluorescence spectrum is also predicted at 2.2 eV to result from CT emission from the eq-ax conformer. Such second band is not observed for **PTeZ-DBPHZ-PTeZ**, however. The behavior stems from the fact that the donor unit of the eq-ax Se compound undergoes planarization in the S_1 state (Figure S15), resulting in a lower energy CT state that is further strongly stabilized by a polarizable environment.^[41] Such planarization is not seen in the Te compounds, for which the S_1 emission energy in the eq-ax conformer is much larger (2.81 eV, Figure 7e).

Phosphorescence energies calculated for both D-A-D compounds are also very similar and predicted to lie around 2.0 eV. This is due to the fact that T_1 states in the ax-ax conformation of both molecules correspond to localized excitations in the acceptor unit. For the pure **PSeZ** and **PTeZ** donor

fragments, phosphorescence energies are predicted at 2.3 eV and 1.9 eV, respectively (Table S13). As such, the experimentally observed similarity in phosphorescence energies between the Te-containing D-A-D compound and the **PTeZ** fragment does not necessarily imply that phosphorescence in **PTeZ-DBPHZ-PTeZ** stems from the donor unit.

Spin-orbit coupling calculations have also been performed for all molecules in toluene using the T_1 geometry. Results are shown in Figure 7. These calculations reveal that S_0 - T_1 spin-orbit couplings are affected mostly by substitution of the Se atoms for Te rather than by conformation. This can be seen from the overall larger couplings calculated for **PTeZ-DBPHZ-PTeZ** conformers when compared to **PSeZ-DBPHZ-PSeZ**. For the ax-ax conformation, which is the most likely to be present, S_1 - T_1 couplings are found to be around 0.7 cm^{-1} for both molecules. The S_1 - T_1 transition in this conformer is allowed, partially due to the fact that it corresponds to a transition between two different LE states (n - π^* and π - π^*).

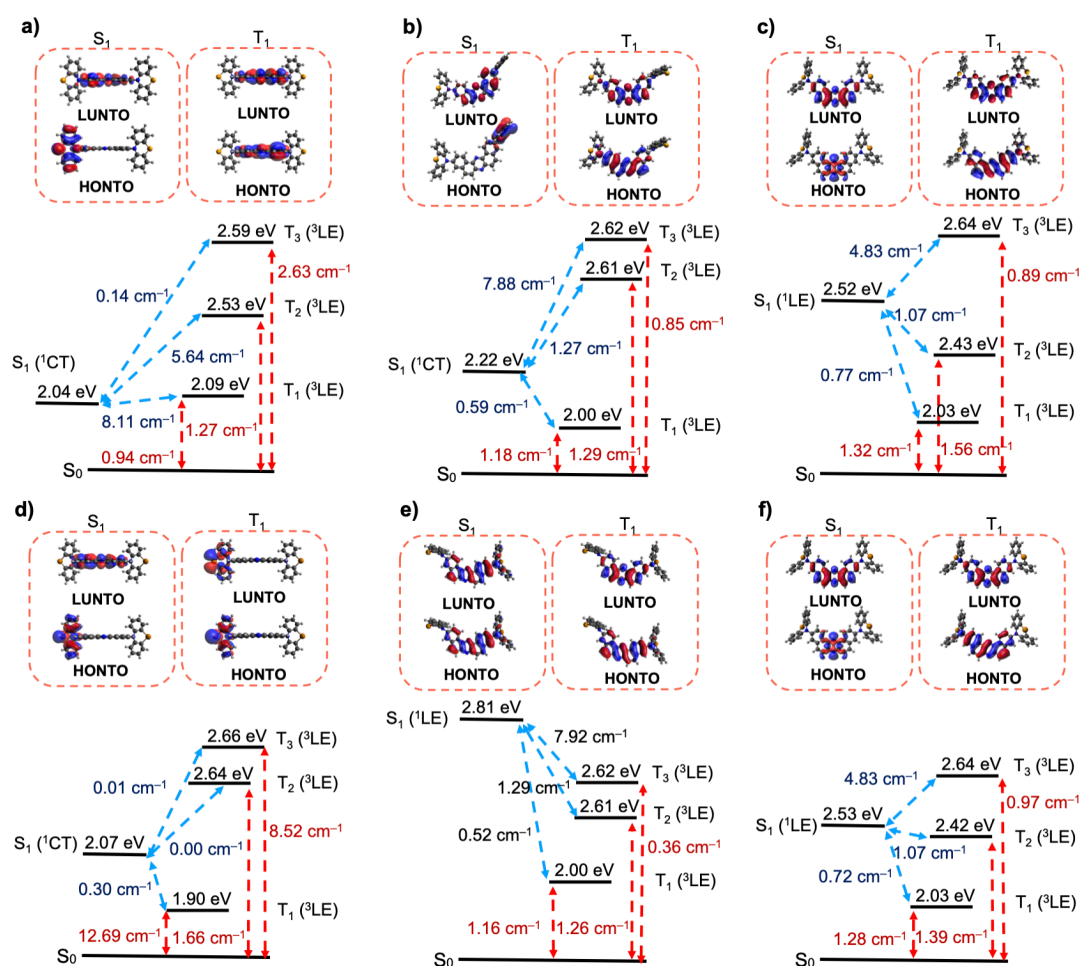


Figure 7. Natural transition orbitals (NTOs) for the S_1 and T_1 states along with corresponding energy levels for the three conformations of a) eq-eq, b) eq-ax, and c) ax-ax conformers of **PSeZ-DBPHZ-PSeZ** in toluene; d) eq-eq, e) ax-eq, and f) ax-ax conformers of **PTeZ-DBPHZ-PTeZ** in toluene; Blue and red arrows correspond to the spin-orbit couplings (SOCs) between S_1 - T_n and T_n - S_0 , respectively.

Conclusion

In conclusion, we have developed a new family of photofunctional dibenzo[*a,j*]phenazine-cored twisted donor–acceptor–donor (D–A–D) compounds having Se and Te bridging atoms in the electronic donors. Of the developed compounds, selenium-containing D–A–D compound **PSeZ-DBPHZ-PSeZ** displays unique multi-photofunctionality of polymorph-dependent multi-photoluminescence, single molecular white emission, various external-stimuli-responsive luminochromism, and unusual dual emission of fluorescence and room-temperature phosphorescence in thin films and OLED devices. In contrast, the tellurium analogue **PTeZ-DBPHZ-PTeZ** are non-emissive in the solid states, probably due to the accelerated ISC and the following IC. Despite the quenching in the condensed phase, the tellurium compound shows RTP in host matrices and OLED devices. Also, unexpectedly we have found out that the donor **PTeZ** represents a new family of RTP-displaying organotellurium compounds.

From the careful comparison of the organoselenium/tellurium compounds with the lighter chalcogen analogues, the most striking effect of replacing with Se and Te for S in the DBPHZ-cored D–A–D twisted scaffold involves the drastic increase in the preference of ax-oriented conformers over the eq ones, due to transannular electronic interaction. This conformational change strongly affects the absorption and photoluminescence profiles in solutions, the reversibility in external-stimuli-induced phase transition, and excited states energy parameters such as ΔE_{ST} , ΔE_{TT} , and spin-orbit coupling (SOCs) that govern the fate of the mechanisms involved in the excited states. The knowledge obtained through the knowledge would pave the new avenue for multi-photofunctional organoselenium and organotellurium materials.

Acknowledgements

Y.T. acknowledges a Grant-in-Aid for Scientific Research on Innovative Areas “ π -System Figuration: Control of Electron and Structural Dynamism for Innovative Functions” (JSPS KAKENHI Grant Number JP15H00997 & JP17H05155) and “Aquatic Functional Materials: Creation of New Materials Science for Environment-Friendly and Active Functions” (JSPS KAKENHI Grant Number JP19H05716) from the MEXT (Ministry of Education, Culture, Science and Technology, Japan), a Grant-in-Aid for Scientific Research (B) (JSPS KAKENHI Grant Number JP20H02813), and the Research Grant from the Japan Prize Foundation, and the Continuation Grants for Young Researchers from the Asahi Glass Foundation, and the Research Grant in the Natural Science from the Mitsubishi Foundation. Y.T. and S.M. acknowledge NIPPOH CHEMICALS for supplying *N,N*-diiodo-5,5-dimethylhydantoin (DIH). P. de S. and L. E. de S. acknowledge support by a research grant (00028053) from VILLUM FONDEN. P.D. and N.O.D. acknowledges the Polish National Science Centre funding, grant no. 2018/31/B/ST5/03085. P.D. and N.O.D. acknowledges the supporting awards from the Rector of the Silesian University of Technology (04/040/BKM20/0124, 04/040/RGJ21/0149). Y.T.,

N.O.D., P. de S. and P.D. acknowledge the EU's Horizon 2020 for funding the OCTA project under grant agreement No 778158.

Keywords: selenium • tellurium • room-temperature phosphorescence • mechanochromism • organic light-emitting diodes

- [1] a) C. W. Nogueira, G. Zeni, J. B. T. Rocha, *Chem. Rev.* **2004**, *104*, 6255–6285; b) B. Banerjee, M. Koketsu, *Coor. Chem. Rev.* **2017**, *339*, 102–127; c) *Organoselenium Compounds in Biology and Medicine: Synthesis, Biological and Therapeutic Treatments* (Eds.: V. K. Jain, K. I. Priyadarsini), The Royal Society of Chemistry, Croydon, UK, **2018**; d) T. Wirth, *Angew. Chem.* **2015**, *127*, 10212–10214; *Angew. Chem. Int. Ed.* **2015**, *54*, 10074–10076.
- [2] a) M. R. Detty, A. E. Friedman, A. R. Oseroff, *J. Org. Chem.* **1994**, *59*, 8245–8250; b) Z. Chen, H. Lai, L. Hou, T. Chen, *Chem. Commun.* **2020**, *56*, 179–196.
- [3] a) S. T. Manjare, Y. Kim, D. G. Churchill, *Acc. Chem. Res.* **2014**, *47*, 2985–2998; b) S. Panda, A. Panda, S. S. Zade, *Coord. Chem. Rev.* **2015**, *300*, 86–100.
- [4] a) L Engman, *Acc. Chem. Res.* **1985**, *18*, 274–279; b) *The Chemistry of Organic Selenium and Tellurium Compounds, Vol. 3* (Ed.: Z. Rappoport), Wiley-VCH, Weinheim, **2012**.
- [5] a) M R. Detty, F. Zhou, A. E. Friedman, *J. Am. Chem. Soc.* **1996**, *118*, 313–318; b) M. Oba, Y. Okada, K. Nishiyama, W. Ando, *Org. Lett.* **2009**, *11*, 1879–1881; c) E. A. Alberto, L. M. Muller, M. R. Detty, *Organometallics* **2014**, *33*, 5571–5581; d) Y. Okada, M. Oba, A. Arai, K. Tanaka, K. Nishiyama, W. Ando, *Inorg. Chem.* **2010**, *49*, 383–385; e) M Godoi, M. W. Paixão, A. L. Braga, *Dalton Trans.* **2011**, *40*, 11347–11355; f) V. Rathore, C. Jose, S. Kumar, *New. J. Chem.* **2019**, *43*, 8852–8864.
- [6] a) J. Xia, T. Li, C. Lu, H. Xu, *Macromolecules* **2018**, *51*, 7435–7455; b) S. Yamago, *Bull. Chem. Soc. Jpn.* **2020**, *93*, 287–298.
- [7] a) L. V. Romashov, V. P. Ananikov, *Chem. Eur. J.* **2013**, *19*, 17640–17660; b) L. Wang, W. Cao, H. Xu, *ChemNanoMat* **2016**, *2*, 479–488; c) W. Cao, H. Xu, *Mater. Chem. Front.* **2019**, *3*, 2010–2017.
- [8] a) K. Selvakumar, H. B. Singh, *Chem. Sci.* **2018**, *9*, 7027–7042; b) M. Fourmigué, A. Dhaka, *Coord. Chem. Rev.* **2020**, *403*, 213084/1–17; c) N. Biot, D. Bonifazi, *Coord. Chem. Rev.* **2020**, *413*, 213243/1–22
- [9] a) T. Otsubo, K. Takimiya, In *Handbook of Thiophene-Based Materials: Applications in Organic Electronics and Photonics* (Eds.: I. F. Perpepichka, D. F. Perepichka), John Wiley & Sons Ltd, Chichester, UK, pp 321–340, **2009**; b) L. Zhang, S. M. Fakhouri, F. Liu, J. C. Timmons, N. A. Ran, A. L. Briseno, *J. Mater. Chem.* **2011**, *21*, 1329–1337; c) T. Okamoto, M. Mitani, C. P. Yu, C.

- Mitsui, M. Yamagishi, H. Ishii, G. Watanabe, S. Kumagai, D. Hashizume, S. Tanaka, M. Yano, T. Kushida, H. Sato, K. Sugimoto, T. Kato, J. Takeya, *J. Am. Chem. Soc.* **2020**, *142*, 14974–14984.
- [10] a) J. G. Manion, J. R. Panchuk, D. S. Seferos, *Chem. Rec.* **2019**, *19*, 1113–1122; b) M. Jeffries-EL, B. M. Kobilka, B. J. Hale, *Macromolecules* **2014**, *47*, 7253–7271.
- [11] S. A. Gregory, A. K. Menon, S. Ye, D. S. Seferos, J. R. Reynolds, S. K. Yee, *Adv. Energy Mater.* **2018**, *8*, 1802419/1–8.
- [12] C. C. Hoover, D. S. Seferos, *Chem. Sci.* **2019**, *10*, 9182–9188.
- [13] K. Wittel, R. Manne, *Theoret. Chim. Acta (Berl.)* **1974**, *33*, 347–349.
- [14] M. A. El-Sayde, *Acc. Chem. Res.* **1968**, *1*, 8–16.
- [15] R. D. Pensack, Y. Song, T. M. McCormick, A. A. Jahnke, J. Hollinger, D. S. Seferos, G. D. Scholes, *J. Phys. Chem. B* **2014**, *118*, 2589–2597.
- [16] D. de Sa Pereira, D. R. Lee, N. A. Kukhta, K. H. Lee, C. L. Kim, A. S. Batsanov, J. Y. Lee, A. P. Monkman, *J. Mater. Chem. C* **2019**, *7*, 10481–10490.
- [17] B. H. Drummond, G. C. Hoover, A. J. Gillett, N. Aizawa, W. K. Myers, B. T. McAllister, S. T. E. Jones, Y.-J. Pu, D. Credgington, D. S. Seferos, *J. Phys. Chem. C* **2020**, *124*, 6364–6370.
- [18] D. R. Lee, K. H. Lee, W. Shao, C. L. Kim, J. Kim, J. Y. Lee, *Chem. Mater.* **2020**, *32*, 2583–2592.
- [19] a) Y. Tao, K. Yuan, T. Chen, P. Xu, H. Li, R. Chen, C. Zheng, L. Zhang, W. Huang, *Adv. Mater.* **2014**, *26*, 7931–7958; b) F. B. Dias, T. J. Penfold, A. P. Monkman, *Methods Appl. Fluoresc.* **2017**, *5*, 012001; c) Z. Yang, Z. Mao, Z. Xie, Y. Zhang, S. Liu, J. Zhao, J. Xu, Z. Chi, M. P. Aldred, *Chem. Soc. Rev.* **2017**, *46*, 915–1016; d) M. Y. Wong, E. Zysman-Colman, *Adv. Mater.* **2017**, *29*, 1605444; e) M. Sarma, K.-T. Wong, *ACS Appl. Mater. Interfaces* **2018**, *10*, 19279–19304; f) X. K. Chen, D. Kim, J.-L. Brédas, *Acc. Chem. Res.* **2018**, *51*, 2215–2224; g) Y. Liu, C. Li, Z. Ren, X. Yan, M. R. Bryce, *Nat. Rev. Mater.* **2018**, *3*, 18020.
- [20] a) S. Mukherjee, P. Thilagar, *Chem. Commun.* **2015**, *51*, 10988–11003; b) M. Baroncini, G. Bergamini, P. Ceroni, *Chem. Commun.* **2017**, *53*, 2081–2093; c) P. Ceroni, *Chem.* **2016**, *1*, 522–530; d) A. Forni, E. Lucenti, C. Botta, E. Cariati, *J. Mater. Chem. C* **2018**, *6*, 4603–4626; e) H. Yuasa, S. Kuno, *Bull. Chem. Soc. Jpn.* **2018**, *91*, 223–229; f) G. Zhan, Z. Liu, Z. Bian, C. Huang, *Front. Chem.* **2019**, *7*, 305/1–6; g) H. Ma, A. Lv, S. Wang, Z. An, H. Shi, W. Huang, *Ann. Phys. (Berlin)* **2019**, *531*, 1800482/1–14.
- [21] H. Chen, Y. Deng, X. Zhu, L. Wang, L. Lv, X. Wu, Z. Li, Q. Shi, A. Peng, Q. Peng, Z. Shuai, Z. Zhao, H. Chen, H. Huang, *Chem. Mater.* **2020**, *32*, 4038–4044.
- [22] L. Xu, K. Zhou, H. Ma, A. Lv, D. Pei, G. Li, Y. Zhang, Z. An, A. Li, G. He, *ACS Appl. Mater. Interfaces* **2020**, *12*, 18385–18394.

- [23] a) Y. Sagara, T. Kato, *Nat. Chem.* **2009**, *1*, 605–610; b) A. Pucci, R. Bizzarri, G. Ruggeri, *Soft Matter* **2011**, *7*, 3689–3700; c) Z. Chi, X. Zhang, B. Xu, X. Zhou, C. Ma, Y. Zhang, S. Liu, J. Xu, *Chem. Soc. Rev.* **2012**, *41*, 3878–3896; d) Z. Ma, Z. Wang, M. Geng, Z. Xu, X. Jia, *ChemPhysChem* **2015**, *16*, 1811–1828; e) Y. Sagara, S. Yamane, M. Mitani, C. Weder, T. Kato, *Adv. Mater.* **2016**, *28*, 1073–1095; f) S. Xue, X. Qiu, Q. Sun, W. Yang, *J. Mater. Chem. C* **2016**, *4*, 1568–1578; g) P. Xue, J. Ding, P. Wang, R. Lu, *J. Mater. Chem. C* **2016**, *4*, 6688–6706; h) C. Wang, Z. Li, *Mater. Chem. Front.* **2017**, *1*, 2174–2194.
- [24] a) P. Data, Y. Takeda, *Chem. Asian J.* **2019**, *14*, 1613–1636; b) Y. Takeda, P. Data, S. Minakata, *Chem. Commun.* **2020**, 56, 8884–8894.
- [25] P. Data, P. Pander, M. Okazaki, Y. Takeda, S. Minakata, A. P. Monkman, *Angew. Chem. Int. Ed.* **2016**, *55*, 5739–5744; *Angew. Chem.* **2016**, *128*, 5833–5838.
- [26] a) M. Okazaki, Y. Takeda, P. Data, P. Pander, H. Higginbotham, A. P. Monkman, S. Minakata, *Chem. Sci.* **2017**, *8*, 2677–2686; b) P. Data, M. Okazaki, S. Minakata, Y. Takeda, *J. Mater. Chem. C* **2019**, *7*, 6616–6621; c) Y. Takeda, H. Mizuno, Y. Okada, M. Okazaki, S. Minakata, T. Penfold, G. Fukuhara, *ChemPhotoChem* **2019**, *3*, 1203–1211.
- [27] Y. Takeda, T. Kaihara, M. Okazaki, H. Higginbotham, P. Data, N. Tohnai, S. Minakata, *Chem. Commun.* **2018**, *54*, 6847–6850.
- [28] H. Yamagishi, S. Nakajima, J. Yoo, M. Okazaki, Y. Takeda, S. Minakata, K. Albrecht, K. Yamamoto, I. Badía-Domínguez, M. M. Oliva, M. C. R. Delgado, Y. Ikemoto, H. Sato, K. Imoto, K. Nakagawa, H. Tokoro, S.-i. Ohkoshi, Y. Yamamoto, *Commun. Chem.* **2020**, *3*, 118/1–8.
- [29] H. F. Higginbotham, M. Okazaki, P. de Silva, S. Minakata, Y. Takeda, P. Data, *ACS Appl. Mater. Interfaces* **2021**, *13*, 2899–2907.
- [30] a) S. Izumi, H. F. Higginbotham, A. Nyga, P. Stachelek, N. Tohani, P. de Silva, P. Data, Y. Takeda, S. Minakata, *J. Am. Chem. Soc.* **2020**, *142*, 1482–1491; b) A. Nyga, S. Izumi, H. F. Higginbotham, P. Stachelek, S. Pluczyk, P. de Silva, S. Minakata, Y. Takeda, P. Data, *Asian J. Org. Chem.* **2020**, *9*, 2153–2161; c) S. Izumi, A. Nyga, P. de Silva, N. Tohnai, S. Minakata, P. Data, Y. Takeda, *Chem. Asian J.* **2020**, *15*, 4098–4103.
- [31] Y. Takeda, M. Okazaki, S. Minakata, *Chem. Commun.* **2014**, *50*, 10291–10294.
- [32] T. Junk, K. J. Irgolic, *Heterocycles* **1989**, *28*, 1007–1013.
- [33] C. Cremer, M. Goswami, C. K. Rank, B. de Bruin, F. W. Patureau, *Angew. Chem. Int. Ed.* doi.org/10.1002/anie.202015248; *Angew. Chem.* doi.org/10.1002/ange.202015248.
- [34] H. Naito, Y. Morisaki, Y. Chujo, *Angew. Chem. Int. Ed.* **2015**, *54*, 5084–5087; *Angew. Chem.* **2015**, *127*, 5173–5176.
- [35] G. te Velde, F. M. Bickelhaupt, E. J. Baerends, C. F. Guerra, S. J. A. van Gisbergen, J. G. Snijders, T. Ziegler, *J. Comput. Chem.* **2001**, *22*, 931–967.

- [36] Z. Chen, C.-L. Ho, L. Wang, W. Y. Wong, *Adv. Mater.* **2020**, 32, 1903269/1–45.
- [37] a) G. He, W. T. Delgado, D. J. Schatz, C. Merten, A. Mohammadpour, L. Mayr, M. J. Ferguson, R. McDonald, A. Brown, K. Shankar, E. Rivard, *Angew. Chem. Int. Ed.* **2014**, 53, 4587–4591; *Angew. Chem.* **2014**, 126, 4675–4679; b) A. Kremer, C. Aurisicchio, F. de Leo, B. Ventura, J. Wouters, N. Armaroli, A. Barbieri, D. Bonifazi, *Chem. Eur. J.* **2015**, 21, 15377–15387; c) L. Xu, G. Li, T. Xu, W. Zhang, S. Zhang, S. Yin, Z. An, G. He, *Chem. Commun.* **2018**, 54, 9226–9229; d) M. Jiang, J. Guo, B. Liu, Q. Tan, B. Xu, *Org. Lett.* **2019**, 21, 8328–8333.
- [38] M. Lapkowski, R. Motyka, J. Suwiński, P. Data, *Macromol. Chem. Phys.* **2012**, 213, 29–35.
- [39] $IP = (5.1 + {}^{\text{ox}}E_{\text{onset}}/V)$ [eV]; $EA = (5.1 + {}^{\text{red}}E_{\text{onset}}/V)$ [eV]. a) C. M. Cardona, W. Li, A. E. Kaifer, D. Stockdale, G. Bazan, *Adv. Mater.* **2011**, 23, 2367–2371; b) J.-L. Bredas, *Mater. Horiz.* **2014**, 1, 17–19.
- [40] M. Shimizu, T. Sakurai, *ChemPlusChem* **2020**, 86, 446–459.
- [41] P. de Silva, *J. Phys. Chem. Lett.* **2019**, 10, 5674–5679.